Spatiotemporal transformation of dissolved organic matter along an alpine stream flowpath on the Qinghai-Tibetan Plateau: importance of source and permafrost degradation

Yinghui Wang [a,b], Robert G.M. Spencer [c], David C. Podgorski [d], Anne M. Kellerman [c], Harunur Rashid [a], Phoebe Zito [d], Wenjie Xiao [b], Dandan Wei [a], Yuanhe Yang [e], Yunping Xu [a*]

[a] *Shanghai Engineering Research Center of Hadal Science and Technology*, *College of Marine Sciences, Shanghai Ocean University, Shanghai 201306, China.*

[b] *Key Laboratory for Earth Surface Processes of the Ministry of Education, College of Urban and Environmental Sciences, Peking University, Beijing 100871, China.*

[c] *National High Magnetic Field Laboratory Geochemistry Group and Department of Earth, Ocean, and Atmospheric Science, Florida State University, Tallahassee, FL 32306, USA*

[d] *Pontchartrain Institute for Environmental Sciences, Department of Chemistry, University of New Orleans, New Orleans, LA, 70148, USA*

[e] *State Key Laboratory of Vegetation and Environmental Change, Institute of Botany, Chinese Academy of Sciences, Beijing 100093, China*

*Corresponding author. *E-mail*: ypxu@shou.edu.cn (Y. Xu)

Abstract The Qinghai-Tibetan Plateau (QTP) accounts for approximately 70% of global alpine permafrost and is an area sensitive to climate change. The thawing and mobilization of ice and organic carbon-rich permafrost impact hydrologic conditions and biogeochemical processes on the QTP. Despite numerous studies of Arctic permafrost, there are no reports to date for the molecular-level in-stream processing of permafrost-derived dissolved organic matter (DOM) on the QTP. In this study, we examine temporal and spatial changes of DOM along an alpine stream (3850–3207 m above sea level) by Fourier transform ion cyclotron resonance mass spectrometry (FT-ICR MS), accelerator mass spectrometry (AMS) and UV-visible spectroscopy. Compared to downstream sites, dissolved organic matter (DOM) at the headstream site exhibited older radiocarbon age, higher mean molecular weight, higher aromaticity and fewer highly unsaturated compounds. At the molecular level, 6409 and 1345 formulas were identified as unique to the active layer (AL) leachate and permafrost layer (PL) leachate, respectively. Comparing permafrost leachates to the downstream site, 59% of AL-specific formulas and 90% of PL-specific formulas were degraded, likely a result of rapid instream degradation of permafrost-derived DOM. From peak discharge in the summer to low flow in late autumn, the DOC concentration at the headstream site decreased from 13.9 to 10.2 mg/L, while the ^{14}C age increased from 745 to 1560 years before present (BP), reflecting an increase in the relative contribution of deep permafrost carbon due to the effect of changing hydrological conditions over the course of the summer on DOM source (AL vs. PL). Our study thus demonstrates that hydrological conditions impact the mobilization of permafrost carbon in an alpine fluvial network, the signature of which is quickly lost through instream mineralization and transformation.

Keywords: dissolved organic matter; permafrost; Qinghai-Tibet Plateau; FT-ICR MS;

radiocarbon age

1. INTRODUCTION

The amount of organic carbon stored in permafrost is roughly twice as much as that in the atmosphere and represents the largest component of the terrestrial carbon pool (Zimov et al., 2006; Tarnocai et al., 2009). Accelerated climate warming has led to a succession of changes associated with permafrost thaw, where water once frozen in permafrost soils has changed watershed hydrology, topography and ecosystem biogeochemistry (Frey and Smith, 2005; Abbott et al., 2015; Vonk et al., 2015). When permafrost-derived organic carbon enters aquatic systems, it can be rapidly mineralized and transformed by microbes and light (Cory et al., 2014; Drake et al., 2015; Vonk et al., 2015). Therefore, the mobilization of organic carbon from permafrost soils where it has been relatively stable for thousands of years into dissolved carbon could increase greenhouse gas emissions (Cory et al., 2013; Vonk et al., 2013; Mann et al., 2015; Ward and Cory, 2016; Selvam et al., 2017) and exacerbate climate warming via a positive feedback loop (Koven et al., 2011; Schuur et al., 2015).

The seasonal thawing-freezing cycle of permafrost soils could change hydrologic conditions and restrict source water contributions to river flow, leading to variability in the flux and the chemical composition of dissolved organic matter (DOM) in permafrost-impacted watersheds (Petrone et al., 2006; Laudon et al., 2011). DOM in the Yukon River exhibits seasonal changes in aromaticity, molecular weight, ^{14}C age and biodegradability (Striegl et al., 2007; Spencer et al., 2008; Wickland et al., 2012; O'Donnell et al., 2014). Since the persistence of DOM in aquatic systems is related to its chemical composition (Kellerman et al., 2015; Kellerman et al., 2018), detailed chemical characterization of DOM is essential to illustrate the environmental behavior

and the fate of seasonally exported permafrost organic carbon.

The Qinghai-Tibet Plateau (QTP), the world's largest and highest plateau, plays a critical role in the evolution of the Asian Monsoon (Sato and Kimura, 2007; Wu et al., 2007) and supplies water to several large rivers such as the Yangtze River, Yellow River and Yarlung Tsangpo (Yao et al., 2007; Kang et al., 2010). As a climate sensitive region, the QTP has experienced significant warming since the 1950s (Qiu, 2008) with the mean annual air temperature rising at a rate of 0.36 °C per decade from 1961 to 2007 (Wang et al., 2008). Consequently, permafrost soils on the QTP have begun to thaw and collapse, causing abundant organic carbon loss from in-situ degradation (Mu et al., 2016) and relocation (e.g., selective leaching in different soil layers; Wang et al,. 2018). However, compared with an abundance of studies on Arctic permafrost, biogeochemical studies on QTP permafrost are scant. This results in a limited understanding of the permafrost carbon cycle as a whole since the QTP represents nearly 10% of global permafrost, furthermore, the QTP differs from the Arctic in altitude, climate, and hydrology (Bockheim and Munroe, 2014).

Here, we conducted a study on the spatial and temporal change of permafrost-derived DOM on the northeastern QTP. We applied multiple analytical techniques including Fourier transform ion cyclotron resonance mass spectrometry (FT-ICR MS), AMS radiocarbon analyses (^{14}C), and UV-visible optical spectroscopy. Our objective was two-fold: 1) determine the dominant sources of alpine stream DOM on the QTP (active layer (AL) vs. permafrost layer (PL)); and 2) trace the persistence and degradation of permafrost-derived DOM in an alpine fluvial network. This work represents the first step in characterizing in-stream removal and transformation processes of permafrost organic carbon at the molecular level on the QTP.

2. MATERIALS AND METHODS

2.1. Study area and sampling

Our study area is located in Gangcha County, north of Qinghai Lake. The climate is a typical plateau continental climate, characterized by extensive solar duration (~3000 hours per year), long cold and dry winters, and short cool and humid summers (Peng et al., 2015). During 2013-2016, January had the lowest average monthly temperature (–11.82 °C), while December had the lowest average monthly precipitation (0.3 mm). Meanwhile, the highest average monthly temperature and precipitation occurred in July (11.66 °C) and August (124.67 mm), respectively. These climate data are available at http://data.cma.cn. The permafrost soil in the region was developed in the late Quaternary, and accumulated > 2 m thick in mountainous areas of the Gangcha County. Due to rapid climate warming on the QTP, the ice-rich permafrost has begun to thaw, and several thermo-erosion gullies formed a decade ago. In this study, we focused on a continuous system that starts with a thermo-erosion gully (> 200 m long), forms a stream which flows into Qinghai Lake, the largest lake in China with a surface area of ca. 4500 km^2. Thawed permafrost slumping exposed soil profiles at the gully heads (ca. 3850 meters above sea level; masl); detailed description on the collapse can be found in Wang et al. (2018). The top 60 cm is AL that comprises abundant grass litter and roots, underlain by dark PL without visible plant debris. The maximal thaw depth reached 78 cm in August 2015 (i.e. thawing into the PL). Seasonal thaw of the entire AL and the upper PL allows for both vertical and lateral percolation of rainwater, which mobilizes large amounts of particulate and dissolved organic matter. The water in the gully flows southward across the hillslope before draining into Qinghai Lake, and the total length of the stream is around 40 km (Fig. 1).

Our fieldwork was conducted in the summer and autumn of 2015 and 2016. In

2015, a time-series sampling campaign was conducted at the headstream (Q-1) from August 1st when the warm and humid climate caused the largest export of leachates, to October 15th when the leaching ceased due to little precipitation and low temperature. On August 1st of 2015 and 2016, AL and PL leachates were collected at depths of 60 cm and 220 cm, respectively, at the gullies' head. 20 L HDPE carboys were cleaned with pure water, 0.1 N hydrochloric acid and pure water again prior to use. It typically took two days to gather > 15 L of leachate waters. After that, the leachate samples were immediately kept on ice and in the dark. They were transported to a temporary laboratory in Gangcha County within 6 hours. Besides soil leachates, water samples (20 L each) were collected from twenty sites along the stream (Fig. 1). Sampling sites Q-1 to Q-10 are located in a first-order stream (ca. 8.5 km long) that originates in the largest thermo-erosion gully, whereas sites Q-11 and Q-12 are located in another first-order stream nearby (ca. 6.9 km long). These two streams merge together to form the main stream, along which sampling sites Q-13 to Q-20 were located. Surface water samples were collected using pre-cleaned HDPE carboys and kept on ice and in the dark until filtering through Whatman GF/F filters (0.7 μm) within 6 hours after sampling. To obtain enough carbon for ^{14}C analyses, aliquots of the 0.7 μm filtrate were concentrated over a cross-flow ultrafiltration system with a 1 kDa cut off (Millipore®, Pellicon 2 system). The retentates and the remaining filtrate were all stored at –20 ºC until further analysis. All glassware and GF/F filters were combusted at 450 ºC for at least 4 hours prior to use.

2.2. Hydrological condition, DOC concentration and optical absorbance in alpine streams

On Aug. 1st 2015, stream water temperature, pH and conductivity were measured

with a portable Horiba W-23XD Water Quality Monitoring System. A portable propeller-type current meter was used to measure the flow rate at the stream cross-section, 5–9 measurements were performed. The water flux was calculated according to average flow rate and cross-sectional area of the stream. The DOC concentration of each water sample was determined by 3-5 injections on a Shimadzu TOC-V_{CPH} analyzer using high temperature combustion, and the coefficient of variance across measurements was < 2%.

The optical properties of the water samples were determined using a Shimadzu UV-1800 spectrophotometer. The scan range was between 200 and 800 nm and Milli-Q water (18.2 MΩ cm^{-1}) was used as the blank. A quartz cell with 1.0 cm pathlength was used. The spectral slope of the 275–295 nm region ($S_{275-295}$), an indicator for the molecular weight of DOM (Helms et al., 2008), was determined by applying log linear fits across the wavelengths 275–295 nm. Specific UV absorbance ($SUVA_{254}$), an indicator for relative aromatic C content, was calculated by dividing the decadic UV absorbance at 254 nm with DOC concentration (Weishaar et al., 2003).

2.3. Electrospray ionization Fourier transform ion cyclotron resonance mass spectrometry (ESI FT-ICR MS)

Selected water samples collected in 2016 from headstream (Q-1), mid-stream (Q-9), and downstream (Q-17), as well as leachate samples collected from the AL and PL, were prepared for FT-ICR MS analyses. They were solid-phase extracted (SPE) using Bond Elut PPL (Agilent Technologies, 100 mg PPL in 3 mL cartridge), following the procedures of Dittmar et al. (2008). In order to avoid overloading of the SPE column, the aliquot volume of SPE DOM was calculated based on an average SPE recovery (60% for permafrost DOM; Ward et al., 2015) and a final eluate concentration of 40 μg C/mL

(in 2 mL methanol). The methanol extracts were analyzed on a 9.4 tesla custom-built FT-ICR MS at the National High Magnetic Field Laboratory (NHMFL; Tallahassee, FL; Kaiser et al., 2011). The direct infusion flow rate was 0.7 µL/min. A total of 100 broadband scans between m/z 150-2000 were co-added for each mass spectrum. After internal calibration in MIDAS Predator Analysis (NHMFL), formulas were assigned based on published rules to signals > 6σ RMS baseline noise (Stubbins et al., 2010) using EnviroOrg®™ software (Corilo, 2015) and categorized by compound class based on the elemental composition of molecular formulas (Kujawinski, 2002; Stenson et al. 2003; Spencer et al., 2014). Formulas with mass measurement accuracy < 0.4 ppm were assigned within the following compositional constraints: $C_{1\text{-}100}$, $H_{2\text{-}200}$, $O_{1\text{-}30}$, $N_{0\text{-}3}$, $S_{0\text{-}2}$. A modified aromaticity index (AI_{mod}) was calculated according to the definition of Koch and Dittmar (2006): $AI_{mod} = \frac{1+C-0.5O-S-0.5(H+N+P)}{C-0.5O-S-N}$, and if AI_{mod} is negative, then AI=0. The groups referenced in this study are: 1) aliphatics (Ali.): H/C 1.5 - 2.0, O/C < 0.9, N = 0; 2) peptide-like (Pep.): H/C 1.5 - 2.0, O/C < 0.9, N > 0; 3) highly unsaturated compounds (Uns.): AI_{mod} < 0.5, H/C < 1.5; 4) polyphenols (Pol.): 0.5 < AI_{mod} < 0.67; 5) condensed aromatics (CA): $AI_{mod} \geq 0.67$. Some compound groups are ambiguous as the formulae may also occur in alternative isomeric arrangements. The relative abundance of the defined compound class, mean molecular weight and AI_{mod} of each sample were all weighted by relative abundance of signals in each spectrum.

2.4. Radiocarbon analyses

Freeze-dried retentates from 1k Da cutoff ultrafiltration are described as high molecular weight ultrafiltrated dissolved organic matter (HMW UDOM; e.g., Broek et al., 2017). They were fumigated with concentrated hydrochloric acid (12 M) in order to remove inorganic carbon. After that, the samples were analyzed on the Keck Carbon

Cycle Accelerator Mass Spectrometry (AMS) Facility at the University of California, Irvine, USA. Processing blank and sample preparation backgrounds were subtracted. Radiocarbon concentrations are given as conventional ^{14}C age following Stuiver and Reimer (1993).

3. RESULTS

3.1. Hydrology and DOC concentration from headstream to downstream water

Discharge increased along the stream reach, from 0.15 m^3/min at the headstream (Q-1) on August 1st 2015 to 24.14 m^3 /min (Q-19) (Fig. 2). pH increased from 7.4 at Q-1 to 8.2 at Q-4 and remained elevated in the middle and lower stream (7.9 to 8.4). Conductivity was relatively constant from Q-1 to Q-6 (35 to 38 μs/cm), then increased at Q-7 and remained elevated downstream (48 to 60 μs/cm). The DOC concentration was high in headstream waters (e.g., 12.48 ± 1.39 mg/L at Q-1 and 10.22 ± 1.09 mg/L at Q-2; Mean ± AD, same hereafter) and decreased downstream (3.13 ± 0.59 to 5.14 ± 0.20 mg/L from Q-5 to Q-20). The mean DOC concentration of the AL leachates (11.57 ± 0.77 mg/L) was an order of magnitude lower than that of the PL leachates (126.40 ± 14.80 mg/L).

3.2. Optical properties of DOM in leachates and stream waters

Paired t-test based on $S_{275\text{-}295}$ and $SUVA_{254}$ of water samples showed no significant inter-annual variation between years 2015 and 2016 (p = 0.716 and p = 0.321, respectively). The mean $S_{275\text{-}295}$ of 2015 and 2016 samples was (14.49 ± 0.34) × 10^{-3} nm^{-1} for the AL leachates and (18.05 ± 0.94) × 10^{-3} nm^{-1} for the PL leachates. In the stream waters, the $S_{275\text{-}295}$ ranged from 16.05× 10^{-3} to 21.80 × 10^{-3} nm^{-1}, increasing in downstream reaches. The mean $SUVA_{254}$ was 3.53 ± 0.17L mg C^{-1} m^{-1} for the AL

leachates and 0.95 ± 0.10L mg C^{-1} m^{-1} for the PL leachates, and decreased in the stream from Q-1 to Q-11 (2.92 to 1.66 L mg C^{-1} m^{-1}), and then remained low (Fig. 3). A strong negative correlation was found between $SUVA_{254}$ and $S_{275-295}$ for water samples from both years ($R^2 = 0.77$, $P < 0.01$).

3.3. Spatiotemporal change of ^{14}C age of HMW UDOM through fluvial networks

The ^{14}C age of HMW UDOM of the PL leachate was 4145 years BP, which was much older than that of the AL leachate (535 years BP; Fig. 4a). The ^{14}C age of HMW UDOM decreased along the stream from 745 years BP for the headstream water (Q-1) to 160 years BP at Q-19, a site close to Qinghai Lake. Besides apparent spatial variability, the ^{14}C age of HMW UDOM also changed temporally. In 2015, the ^{14}C age of HMW UDOM of the headstream water (Q-1) increased from 745 years BP on August 1st, to 1015 years BP on August 11th and 1560 years BP on September 5th (Fig. 4b).

3.4. FT-ICR MS characterization of SPE-DOM

Compared with the PL leachate, the AL leachate was characterized by higher molecular chemodiversity (14709 vs. 9645 assigned formulae), higher mean molecular weight (498.81 vs. 452.73 Da) and higher AI_{mod} (0.47 vs. 0.30). Molecular-level composition revealed that compounds containing both N and S were only detected in the AL leachates and headstream waters. The AL leachate contained 54.28% highly unsaturated compounds, 27.10% polyphenols and 17.23% condensed aromatic compounds, whereas the proportion of aliphatics and peptide-like compounds was minor (ca. 1.30%). Compared with the AL leachate, the PL leachate comprised a higher proportion of highly unsaturated compounds (74.23%) and aliphatics + peptide-like (10.04%), but a lower proportion of polyphenols (11.33%) and condensed aromatics

(4.32%).

Along the stream (Q-1, Q-9, and Q-17), the molecular chemodiversity, mean molecular weight and modified aromaticity index of SPE-DOM decreased from 14924 to 11074, 510.1 to 486.5 Da and 0.43 to 0.36, respectively (Table 1). The relative abundance of aromatics (condensed aromatics and polyphenols) decreased by 48% (35.7% at Q-1 vs. 18.4% at Q-17), whereas that of highly unsaturated compounds increased by 28% (62.8% at Q-1 vs. 80.3% at Q-17). Aliphatics and peptide-like compounds were minor components of stream DOM (<1.3%) and did not exhibit a downstream trend.

4. DISSCUSSION

4.1. AL leachates as a major source of stream DOM

The UV-visible optical parameters and molecular formulas resolved by FT-ICR MS show that the AL and PL leachates have different chemical compositions (Table 1 and 2). This difference is likely attributed to selective release of aromatic components from AL and carbohydrate/protein components from deep PL during the soil thawing process, which was observed in our previous study (Wang et al., 2018). Since chemical composition impacts the reactivity of DOM (Kellerman et al., 2015), the differing chemical composition between the AL and PL leachates that enter the stream may influence bioavailability (Vonk et al., 2013) and photolability (Stubbins et al., 2017). Thus, distinguishing DOM source is crucial for understanding in-stream biogeochemical processes in permafrost-impacted systems. DOM may originate from a variety of sources including permafrost soil (AL and PL) leaching, in-situ microbial production, and wet deposition from snow and rain. At the headstream site (Q-1), however, the dominant source of DOM is permafrost soil leaching, as short residence

times at the gully head restrict in-stream production and wet deposition is likely negligible due to low DOC concentrations in Tibetan glaciers (0.2-3.3 μg/ml; Spencer et al., 2014). Assuming that headstream DOM is derived only from permafrost soil leaching, we are able to estimate the relative contributions of DOM from the AL and PL.

The mean DOC concentration of the AL leachate based on samples from 2015 and 2016 (11.57 ± 0.77 mg/L) is similar to that of the headstream (Q-1; ca. 12.48 ± 1.39 mg/L), but substantially lower than that of the PL leachates (126.40 ± 14.80 mg/L), supporting a predominance of AL-leachate DOM in stream waters. In addition, the $SUVA_{254}$ is 3.52 ± 0.17 L mg C^{-1} m^{-1} for AL leachates and 0.95 ± 0.10 L mg C^{-1} m^{-1} for PL leachates, whereas the $S_{275\text{-}295}$ is (14.49 ± 0.34) × 10^{-3} nm^{-1} for AL leachates and (18.05 ± 0.94) × 10^{-3} nm^{-1} for PL leachates. Similar optical properties and DOC concentrations between AL-leachates and the headstream water (3.52 ± 0.17 L mg C^{-1} m^{-1} vs 2.92 ± 0.13 L mg C^{-1} m^{-1} for $SUVA_{254}$ and (14.49 ± 0.34) × 10^{-3} nm^{-1} vs (16.05 ± 0.28) × 10^{-3} nm^{-1} for $S_{275\text{-}295}$) support DOM that leaches from the AL dominates stream DOM. Furthermore, the stream water at Q-1 has a ^{14}C age of HMW UDOM of 745 years BP, close to that of the AL leachate (535 years BP), and much younger than that of the PL leachate (4145 years BP). Broek et al. (2017) found that although the ^{14}C age of HMW UDOM was significantly younger than that of bulk DOM from North Central Pacific Ocean, the offset between them is constant in the whole marine system. This result suggests that HMW UDOM can serve as a proxy for bulk DOM. Here we estimate the portion of AL and PL-derived organic carbon by using a binary mixing model based on $\Delta^{14}C$ values of HMW UDOM (Criss, 1999, $\Delta^{14}C$ values can be found in supplementary table S1):

$$\Delta^{14}C_{DOM} = f_{AL} \times \Delta^{14}C_{AL} + f_{PL} \times \Delta^{14}C_{PL}$$

295 $1.0 = f_{AL} + f_{PL}$

296 According to this model, ca. 94% of DOC collected from stream site Q-1 on Aug.
297 1, 2015 originated from the AL (Fig. 6a). Headstream ^{14}C age of HMW UDOM
298 increased from summer to fall (Fig. 4b), reflecting an enhanced contribution of old
299 carbon from the deeper soils (i.e., PL), however, the AL still accounted for ≥ 72% of
300 total DOC exported (Fig. 6a). This binary mixing model may overestimate the
301 contribution of AL to stream DOC since PL-derived DOC may be degraded faster than
302 AL-derived DOC, due to the high biolability of ancient permafrost carbon as shown in
303 Arctic ecosystems (Vonk et al., 2013). Nonetheless, the AL appears as a major
304 contributor to stream DOC in the QTP.

305 Seasonal variation of the ^{14}C age (Fig. 4b) has been previously observed in DOM
306 from high latitude permafrost areas in Alaska (Aiken et al., 2014; O'Donnell et al.,
307 2014), with the most enriched ^{14}C values observed in the spring and becoming more
308 depleted through summer-fall and/or during winter. Our result also shows seasonal
309 variations in the ^{14}C age and optical parameters of headstream DOM. From summer to
310 fall, the $SUVA_{254}$ of stream DOM at Q-1 decreased from 2.79 to 2.36 mg C^{-1} m^{-1},
311 whereas the $S_{275\text{-}295}$ increased from 16.33 × 10^{-3} to 16.96 × 10^{-3} nm^{-1}. These temporal
312 changes indicated that the proportion of aromatic components and high molecular
313 weight compounds decreased with the deepening of the PL. The mean monthly air
314 temperature of Gangcha County, after reaching the maximum in July (ca. 10.5 ºC),
315 decreases to 2.1 ºC in September (data from http://data.cma.cn). As air temperature
316 drops, surface soils freeze earlier than deeper soils, leading to an increase in the relative
317 contribution of deep soil carbon (i.e. PL) to stream DOM, although the DOC
318 concentration in Q-1 decreased from 13.87 mg/L to 10.22 mg/L (Fig. 6b).
319

320 **4.2. Selective removal of DOM along the alpine stream on the QTP**

321 The DOC concentration decreased (12.48 to 3.13 mg/L) from upper to mid-stream
322 (Q-1 to Q-5), which may be attributed to several reasons such as aggregation or
323 precipitation, a dilution effect, and in-stream degradation of DOM. Aggregation or
324 precipitation is likely unimportant in our case because the steep gradient of sampling
325 sites prevents significant sediment and floc deposition on stream bedrocks, although
326 this effect can't be excluded completely. Dilution from groundwater is likely since
327 groundwater discharge sustains baseflow of rivers and streams in the QTP (Ge et al.,
328 2008). Downstream groundwater inputs were further supported by the order of
329 magnitude increase in discharge (1.49 to 24.14 m^3/min) and increase in conductivity
330 (37 to 60 μs/cm). Moreover, downstream DOC concentrations remained about 3.0-4.0
331 mg/L (Q-15 to Q-20), indicative of the low DOC concentrations of groundwater.
332 Conversely, a tributary that originated from another thermo-erosion gully merged into
333 the study stream, however, the different tributaries exhibited similar DOC
334 concentrations (e.g., Q-9 and Q-10 vs. Q-11 and Q-12; Fig. 2d). The similarities in DOC
335 concentrations were attributed to homogeneity in dominant vegetation, soil type and
336 climate, and thus, homogeneity in DOM inputs to the different tributaries in our study
337 area. Therefore, additional tributaries could not explain the spatial pattern of DOC
338 concentration.

339 Despite evident dilution, DOC attenuation could be partly due to in-stream
340 degradation given several lines of evidence from optical properties, radiocarbon age
341 and molecular composition. The UV-visible optical parameters, $S_{275\text{-}295}$ and $SUVA_{254}$,
342 have been widely used to assess molecular weight and aromaticity of DOM,
343 respectively (Weishaar et al., 2003; Helms et al., 2008; Spencer et al., 2009; Mann et
344 al., 2012). A downstream increase for $S_{275\text{-}295}$ regardless of sampling time (Fig. 3a)

reflects selected degradation of high molecular weight compounds, leading to the enrichment of low molecular weight DOM. In addition to $S_{275\text{-}295}$, $SUVA_{254}$ varied from 1.50 to 2.92 L mg C^{-1} m^{-1}, showing a general decrease downstream (Fig. 3b). Lignin, an aromatic biopolymer specific for vascular plants (Hedges et al., 1997), is relatively resistant to biodegradation (Hedges et al., 1985), but highly photo-labile (Lanzalunga and Bietti, 2000). Cory et al. (2014) found that sunlight accounts for 70% to 95% of water column carbon processing in Arctic rivers and lakes. Given strong solar radiation and long sunshine duration (~3000 hours per year) on the QTP (Peng et al., 2015), photo-degradation could be an important pathway for carbon removal in QTP streams. A strong negative correlation between $S_{275\text{-}295}$ and $SUVA_{254}$ ($R^2 = 0.73$, $p < 0.01$) indicates that photodegradation of high molecular weight aromatic compounds (like lignin) may play a role in the decrease of mean molecular weight of DOM along the stream, despite that microbial degradation might also contribute the molecular modification in stream.

Similar to $SUVA_{254}$ and $S_{275\text{-}295}$, the data from FT-ICR MS also show a downstream decrease in aromaticity (AI_{mod}: 0.43 to 0.36) and mean molecular weight of stream DOM (510.0 to 486.5 Da; Table 1). Compared with headstream DOM at Q-1, DOM at Q-9 and Q-17 was characterized by a lower proportion of condensed aromatics and polyphenols and enriched in highly unsaturated compounds (Table 1). The decrease in relative abundance of aromatic compounds is consistent with the reports for the photolability of aromatic formulas within permafrost, river and ocean DOM (Stubbins and Dittmar, 2015; Stubbins et al., 2017).

As discussed in section 4.1, AL is the principal contributor to stream DOM. Thus, tracing AL-derived DOM is paramount in estimating biogeochemical processes of carbon in the stream. FT-ICR MS identified 6409 molecular formulas specific to AL-

370 leachates (i.e. not observed in the PL, Table 2). Through various stream processes, some
371 AL specific formulas were removed from the DOM pool (from 17% by Q-1 up to 59%
372 by Q-17), which accounted for 66% of the aromatic compounds and 51% of the highly
373 unsaturated compounds (Table 2). Molecular formulas containing N and/or S were more
374 labile in the fluvial networks than CHO formulas, with 84% of S-containing formulas
375 and 100% of S and N-containing formulas lost (Table 2). Furthermore, the removal of
376 DOM formulas (ca. 83% of AL-specific formulas, and >95% of AL-specific formulas)
377 occurred in upper and mid-stream (leachates to Q-9). Concurrent with the rapid loss of
378 AL-specific formulas, some new molecular formulas were detected by FT-ICR MS,
379 which was mainly attributed to in-situ production by stream algae/microbes, an import
380 from groundwater and molecular transformation of leachate DOM. The van Krevelen
381 diagram showed that the new products were mainly composed of highly unsaturated
382 molecules (Fig. S1). The addition of new molecular formulas was also reflected by the
383 ^{14}C enrichment in middle and lower-stream (Fig. 3b).
384 Overall, our multiple analyses demonstrate a rapid and selective degradation of
385 stream DOM on the QTP. The attenuation of aromatic compounds and enrichment of
386 highly unsaturated compounds could change the environmental photo- and bio-lability
387 of DOM, increasing relative importance of photodegradation in upper stream and
388 biodegradation in lower stream. The continuous change in chemical properties of DOM
389 along the alpine stream flowpath has a potential to shift the aquatic microbial
390 community since DOM serves as an important energy and nutrient source (Wild et al.,
391 2014).
392
393 **4.3. Prediction of in stream carbon dynamic under continued warming**
394 The DOC concentrations, UV-visible optical parameters and FT-ICR MS data all

suggest that currently, the PL is a minor source to stream DOM (see 4.1). However, the QTP is a sensitive area to climate change, with a rate of air temperature rise that is approximately three times the global rate (Qiu, 2008). According to climate model predictions, spatial average temperatures of the QTP will increase by 0.68–0.98 ºC for the period of 2015–2050 (Zhu et al., 2013), and in 2050, the mean AL thickness on the QTP permafrost will increase by approximately 0.3-0.8 m more than that in 2010 (Zhang and Wu, 2012). With the deepening of the AL, carbon that is currently stable in the PL will be thawed and mobilized into downslope aquatic environments, which inevitably changes the relative proportion of AL vs. PL contributions to stream DOM. Thus, it is important to trace the chemical change of PL leachates along the stream. The PL leachate contained only 1345 formulas unique to the PL leachate in comparison to the AL, accounting for 14% of total assigned formulas (Table 2). Most PL-specific formulas were more biolabile components, e.g. aliphatics and peptide-like assignments (73%), followed by highly unsaturated formulas (23.6%) and aromatics (1.9%). At the downstream site (i.e., Q-17), 90% of these PL-specific molecular formulas were lost, substantially higher than that of AL-specific formulas (59%). Furthermore, the vast majority of PL-specific formulas were lost within < 1 km (Q-1: 83%), whereas only 17% of AL-specific formulas were lost by Q-1 (Table 2). Therefore, the FT-ICR MS data demonstrate that permafrost thaw can trigger a rapid degradation of old organic carbon that was previously frozen in soils for thousands of years (Fig. 3a). This is consistent with findings in Arctic fluvial networks that show the utilization of ancient permafrost carbon in headstream waters was rapid (Mann et al., 2015; Frey et al., 2016). Therefore, we hypothesize that with enhanced leaching of deep soil C under continued warming on the QTP, DOM in alpine streams will be more enriched in biolabile aliphatics/peptides and depleted in photolabile aromatics

Finally, despite substantial in-stream degradation, some old permafrost-derived carbon (i.e., polyphenols and highly unsaturated compounds) could persist downstream. In addition, CO_2 produced by respiration of old DOC could be utilized by stream algae to biosynthesize new DOM with an old carbon age. These effects resulted in a sustained deviation from modern ^{14}C age of HMW UDOM in the alpine stream (e.g., 160 years BP at Q-19), and were even detected in large rivers on the QTP (e.g., Yangtze River and Yellow River; Qu et al., 2017). Thus, under continued warming, a greater quantity of older C may be transported into large watersheds on the QTP, and thereby exert an important role in biogeochemical cycles there since older carbon has different photo and bio-lability from young carbon in AL soils.

5. CONCLUSIONS

Permafrost thaw represents positive feedbacks to climate change, but its carbon alteration and removal mechanism is not well known, particularly for the alpine permafrost such as the QTP. Here we use multiple analytical methods (e.g., FT-ICR MS, radiocarbon and UV-visible spectroscopy) to trace spatial and temporal variability of permafrost DOM along an alpine stream in the northeastern QTP, from which four conclusions have been reached.

1) Presently, the AL is the major source to stream DOM with relatively high aromaticity. This character, combined with strong solar radiation on the QTP, suggests sunlight may be an important driver for DOM removal in alpine fluvial networks, which was corroborated by an almost 60% loss of AL specific formulas from the thermo-erosion gully head to downstream waters.

2) From summer to fall (seasonal permafrost thawing to freezing cycle), the concentrations and chemical composition of stream DOM varied significantly at the

thermo-erosion gully head. Even though the total amount of the leached DOC decreased, the contribution of deep permafrost carbon with lower aromaticity and lower MW increased, reflected by an increase of ^{14}C age of HMW UDOM and a decrease in aromaticity of DOM.

3) Although both the AL and PL leachate DOM underwent rapid degradation in the alpine stream, some components with old ^{14}C age were stable to degradation and could be transported downstream, causing ^{14}C values that were more depleted than modern radiocarbon age downstream in our study, and even in large watersheds as observed in Qu et al. (2017).

4) With deepening of the AL under continued climate warming on the QTP, currently stable PL soils will thaw and release greater amounts of old, aliphatic/peptide-like rich DOM to downstream waters. This change in source and chemical composition will make microbial degradation more important for carbon processing and may shift downstream microbial communities, even in large watershed systems. All these factors should be taken into account when interpreting alpine permafrost carbon dynamics under the amplified warming trend observed on the QTP.

ACKNOWLEDGEMENTS

This work was financially supported by the National Basic Research Program of China (2014CB954001). Y.W. thanks the China Scholarship Council for supporting study in the United States of America as a joint Ph. D. student. We are grateful for Futing Liu, Yanyan Yan, Shangzhe Zhou, Xinyu Zhang for assistance in the field. Rudolf Jaffe and two anonymous reviewers are thanked for constructive comments. FT-ICR MS was supported by NSF (DMR-1157490).

References

Abbott, B.W., Jones, J.B., Godsey, S.E., Larouche, J.R. and Bowden, W.B. (2015) Patterns and persistence of hydrologic carbon and nutrient export from collapsing upland permafrost. Biogeosciences 12, 3725-3740.

Aiken, G.R., Spencer, R.G.M., Striegl, R.G., Schuster, P.F. and Raymond, P.A. (2014) Influences of glacier melt and permafrost thaw on the age of dissolved organic carbon in the Yukon River basin. Global Biogeochem. Cycles 28, 525-537.

Bockheim, J.G. and Munroe, J.S. (2014) Organic Carbon Pools and Genesis of Alpine Soils with Permafrost: A Review. Arct. Antarct. Alp. Res. 46, 987-1006.

Broek, T. A. B., Walker, B. D., Guilderson, T. P., and McCarthy, M. D.(2017) Coupled ultrafiltration and solid phase extraction approach for the targeted study of semi-labile high molecular weight and refractory low molecular weight dissolved organic matter, Marine Chemistry, 194, 146-157.

Corilo, Y.E. (2015) EnviroOrg. Florida State University.

Cory, R.M., Crump, B.C., Dobkowski, J.A. and Kling, G.W. (2013) Surface exposure to sunlight stimulates CO_2 release from permafrost soil carbon in the Arctic. Proc. Natl. Acad. Sci. USA 110, 3429-3434.

Cory, R.M., Ward, C.P., Crump, B.C. and Kling, G.W. (2014) Sunlight controls water column processing of carbon in arctic fresh waters. Science 345, 925-928.

Criss, R.E. (1999) Principles of stable isotope distribution. Oxford University Press, New York.

Dittmar, T., Koch, B., Hertkorn, N. and Kattner, G. (2008) A simple and efficient method for the solid-phase extraction of dissolved organic matter (SPE-DOM) from seawater. Limnol. Oceanogr. Methods 6, 230-235.

Drake, T.W., Wickland, K.P., Spencer, R.G., McKnight, D.M. and Striegl, R.G. (2015) Ancient low-molecular-weight organic acids in permafrost fuel rapid carbon dioxide production upon thaw. Proc. Natl. Acad. Sci. USA 112, 13946-13951.

Frey, K.E. and Smith, L.C. (2005) Amplified carbon release from vast West Siberian peatlands by 2100. Geophys. Res. Lett. 32, doi: 10.1029/2004GL022025.

Frey, K.E., Sobczak, W.V., Mann, P.J. and Holmes, R.M. (2016) Optical properties and bioavailability of dissolved organic matter along a flow-path continuum from soil pore waters to the Kolyma River mainstem, East Siberia. Biogeosciences 13, 2279-2290.

Ge, S., Wu, Q.B., Lu, N., Jiang, G.L. and Ball, L. (2008) Groundwater in the Tibet Plateau, western China. Geophys. Res. Lett. 35, 80-86.

Hedges, J.I., Cowie, G.L., Ertel, J.R., James Barbour, R. and Hatcher, P.G. (1985) Degradation of carbohydrates and lignins in buried woods. Geochim. Cosmochim. Acta 49, 701-711.

Hedges, J.I., Keil, R.G. and Benner, R. (1997) What happens to terrestrial organic matter in the ocean? Org. Geochem. 27, 195-212.

Helms, J.R., Stubbins, A., Ritchie, J.D., Minor, E.C., Kieber, D.J. and Mopper, K. (2008) Absorption spectral slopes and slope ratios as indicators of molecular weight, source, and photobleaching of chromophoric dissolved organic matter. Limnol. Oceanogr. 53, 955-969.

Hodgkins, S.B., Tfaily, M.M., Podgorski, D.C., Mccalley, C.K., Saleska, S.R., Crill, P.M., Rich, V.I., Chanton, J.P. and Cooper, W.T. (2016) Elemental composition and optical properties reveal changes in dissolved organic matter along a permafrost thaw chronosequence in a subarctic peatland. Geochim. Cosmochim. Acta 187, 123-140.

Kaiser, N.K., Quinn, J.P., Blakney, G.T., Hendrickson, C.L. and Marshall, A.G. (2011) A novel 9.4 tesla FTICR mass spectrometer with improved sensitivity, mass resolution,

520 and mass range. J. Am. Soc. Mass Spectrom. 22, 1343-1351.
521 Kang, S., Xu, Y., You, Q., Flügel, W.-A., Pepin, N. and Yao, T. (2010) Review of climate
522 and cryospheric change in the Tibetan Plateau. Environ. Res. Lett. 5, doi:10.1088/1748-
523 9326/1085/1081/015101.
524 Kellerman, A.M., Guillemette, F., Podgorski, D.C., Aiken, G.R., Butler, K.D. and
525 Spencer, R.G.M. (2018) Unifying Concepts Linking Dissolved Organic Matter
526 Composition to Persistence in Aquatic Ecosystems. Environ. Sci. Technol., doi:
527 10.1021/acs.est.1027b05513.
528 Kellerman, A.M., Kothawala, D.N., Dittmar, T. and Tranvik, L.J. (2015) Persistence of
529 dissolved organic matter in lakes related to its molecular characteristics. Nat. Geosci. 8,
530 454-457.
531 Koch, B.P. and Dittmar, T. (2006) From mass to structure: an aromaticity index for high-
532 resolution mass data of natural organic matter. Rapid Commun. Mass Spectrom. 20,
533 926-932.
534 Koven, C.D., Ringeval, B., Friedlingstein, P., Ciais, P., Cadule, P., Khvorostyanov, D.,
535 Krinner, G. and Tarnocai, C. (2011) Permafrost carbon-climate feedbacks accelerate
536 global warming. Proc. Natl. Acad. Sci. U. S. A. 108, 14769-14774.
537 Kujawinski, E.B., (2002). Electrospray ionization fourier transform ion cyclotron
538 resonance mass spectrometry (ESI FT-ICR MS): Characterization of complex
539 environmental mixtures. Environ. Forensics 3, 207-216.
540 Lanzalunga, O. and Bietti, M. (2000) Photo- and radiation chemical induced
541 degradation of lignin model compounds. J. Photochem. Photobiol. B: Biol. 56, 85-108.
542 Laudon, H., Berggren, M., Ågren, A., Buffam, I., Bishop, K., Grabs, T., Jansson, M.
543 and Köhler, S. (2011) Patterns and dynamics of dissolved organic carbon (DOC) in
544 boreal streams: the role of processes, connectivity, and scaling. Ecosystems 14, 880-

545 893.
546 Mann, P.J., Davydova, A., Zimov, N., Spencer, R.G.M., Davydov, S., Bulygina, E.,
547 Zimov, S. and Holmes, R.M. (2012) Controls on the composition and lability of
548 dissolved organic matter in Siberia's Kolyma River basin. J. Geophys. Res. Biogeosci.
549 117, doi:10.1029/2011jg001798.
550 Mann, P.J., Eglinton, T.I., McIntyre, C.P., Zimov, N., Davydova, A., Vonk, J.E., Holmes,
551 R.M. and Spencer, R.G. (2015) Utilization of ancient permafrost carbon in headwaters
552 of Arctic fluvial networks. Nat. Commun. 6, doi:10.1038/ncomms8856.
553 Mu, C., Zhang, T., Zhang, X., Li, L., Guo, H., Zhao, Q., Cao, L., Wu, Q. and Cheng, G.
554 (2016) Carbon loss and chemical changes from permafrost collapse in the northern
555 Tibetan Plateau. J. Geophys. Res. Biogeosci. 121, doi:10.1002/2015JG003235.
556 O'Donnell, J.A., Aiken, G.R., Walvoord, M.A., Raymond, P.A., Butler, K.D.,
557 Dornblaser, M.M. and Heckman, K. (2014) Using dissolved organicmatter age and
558 composition to detect permafrost thaw in boreal watersheds of interior Alaska. J.
559 Geophys. Res. Biogeosci. 119, 2155-2170.
560 Peng, S., Du, Q., Wang, L., Lin, A. and Hu, B. (2015) Long-term variations of
561 ultraviolet radiation in Tibetan Plateau from observation and estimation. Int. J. Climatol.
562 35, 1245-1253.
563 Petrone, K.C., Jones, J.B., Hinzman, L.D. and Boone, R.D. (2006) Seasonal export of
564 carbon, nitrogen, and major solutes from Alaskan catchments with discontinuous
565 permafrost. J. Geophys. Res. Biogeosci. 111, doi:10.1029/2006JG000281.
566 Qiu, J. (2008) The third pole. Nature 454, 393-396.
567 Qu, B., Sillanpää, M., Li, C., Kang, S., Stubbins, A., Yan, F., Aho, K.S., Zhou, F. and
568 Raymond, P.A. (2017) Aged dissolved organic carbon exported from rivers of the
569 Tibetan Plateau. PLoS One 12, e0178166, doi:

570 0178110.0171371/journal.pone.0178166.
571 Sato, T. and Kimura, F. (2007) How does the Tibetan Plateau affect the transition of
572 Indian monsoon rainfall? Mon. Weather Rev. 135, 2006-2015.
573 Schuur, E.A.G., McGuire, A.D., Schadel, C., Grosse, G., Harden, J.W., Hayes, D.J.,
574 Hugelius, G., Koven, C.D., Kuhry, P., Lawrence, D.M., Natali, S.M., Olefeldt, D.,
575 Romanovsky, V.E., Schaefer, K., Turetsky, M.R., Treat, C.C. and Vonk, J.E. (2015)
576 Climate change and the permafrost carbon feedback. Nature 520, 171-179.
577 Selvam, B.P., Lapierre, J.-F., Guillemette, F., Voigt, C., Lamprecht, R.E., Biasi, C.,
578 Christensen, T.R., Martikainen, P.J. and Berggren, M. (2017) Degradation potentials of
579 dissolved organic carbon (DOC) from thawed permafrost peat. Sci. Rep. 7,
580 doi:10.1038/srep45811.
581 Spencer, R.G., Aiken, G.R., Wickland, K.P., Striegl, R.G. and Hernes, P.J. (2008)
582 Seasonal and spatial variability in dissolved organic matter quantity and composition
583 from the Yukon River basin, Alaska. Global Biogeochem. Cycles 22, doi:
584 10.1029/2008GB003231.
585 Spencer, R.G.M., Aiken, G.R., Butler, K.D., Dornblaser, M.M., Striegl, R.G. and
586 Hernes, P.J. (2009) Utilizing chromophoric dissolved organic matter measurements to
587 derive export and reactivity of dissolved organic carbon exported to the Arctic Ocean:
588 a case study of the Yukon River, Alaska. Geophys. Res. Lett. 36, 141-153.
589 Spencer, R.G.M., Guo, W., Raymond, P.A., Dittmar, T., Hood, E., Fellman, J. and
590 Stubbins, A. (2014) Source and biolability of ancient dissolved organic matter in glacier
591 and lake ecosystems on the Tibetan Plateau. Geochim. Cosmochim. Acta 142, 64-74.
592 Stenson, A.C.; Marshall, A.G.; Cooper, W.T., (2003) Exact masses and chemical
593 formulas of individual Suwannee River fulvic acids from ultrahigh resolution
594 electrospray ionization Fourier transform ion cyclotron resonance mass spectra, Anal.

595 Chem. 75, 1275-1284.
596 Striegl, R.G., Dornblaser, M.M., Aiken, G.R., Wickland, K.P. and Raymond, P.A. (2007)
597 Carbon export and cycling by the Yukon, Tanana, and Porcupine rivers, Alaska, 2001–
598 2005. Water Resour. Res. 43, doi:10.1029/2006WR005201.
599 Stubbins, A. and Dittmar, T. (2015) Illuminating the deep: Molecular signatures of
600 photochemical alteration of dissolved organic matter from North Atlantic Deep Water.
601 Mar. Chem. 177, 318-324.
602 Stubbins, A., Mann, P.J., Powers, L., Bittar, T.B., Dittmar, T., McIntyre, C.P., Eglinton,
603 T.I., Zimov, N. and Spencer, R.G.M. (2017) Low photolability of yedoma permafrost
604 dissolved organic carbon. J. Geophys. Res. Biogeosci. 122, 200-211.
605 Stubbins, A., Spencer, R.G.M., Chen, H.M., Hatcher, P.G., Mopper, K., Hernes, P.J.,
606 Mwamba, V.L., Mangangu, A.M., Wabakanghanzi, J.N. and Six, J. (2010) Illuminated
607 darkness: Molecular signatures of Congo River dissolved organic matter and its
608 photochemical alteration as revealed by ultrahigh precision mass spectrometry. Limnol.
609 Oceanogr. 55, 1467-1477.
610 Stuiver, M. and Reimer, P.J. (1993) Extended ^{14}C Data Base and Revised Calib 3. 0 14C
611 Age Calibration Program. Radiocarbon 35, 215-230.
612 Tarnocai, C., Canadell, J.G., Schuur, E.A.G., Kuhry, P., Mazhitova, G. and Zimov, S.
613 (2009) Soil organic carbon pools in the northern circumpolar permafrost region. Global
614 Biogeochem. Cycles 23, doi:10.1029/2008gb003327.
615 Vonk, J.E., Mann, P.J., Davydov, S., Davydova, A., Spencer, R.G.M., Schade, J.,
616 Sobczak, W.V., Zimov, N., Zimov, S., Bulygina, E., Eglinton, T.I. and Holmes, R.M.
617 (2013) High biolability of ancient permafrost carbon upon thaw. Geophys. Res. Lett.
618 40, 2689-2693.
619 Vonk, J.E., Tank, S.E., Bowden, W.B., Laurion, I., Vincent, W.F., Alekseychik, P.,

620 Amyot, M., Billet, M.F., Canario, J., Cory, R.M., Deshpande, B.N., Helbig, M., Jammet,
621 M., Karlsson, J., Larouche, J., MacMillan, G., Rautio, M., Anthony, K.M.W. and
622 Wickland, K.P. (2015) Reviews and syntheses: Effects of permafrost thaw on Arctic
623 aquatic ecosystems. Biogeosciences 12, 7129-7167.
624 Wang, B., Bao, Q., Hoskins, B., Wu, G. and Liu, Y. (2008) Tibetan Plateau warming
625 and precipitation changes in East Asia. Geophys. Res. Lett. 35, 63-72.
626 Wang, Y., Xu, Y., Spencer, R.G.M., Zito, P., Kellerman, A., Podgorski, D., Xiao, W.,
627 Wei, D., Rashid, H. and Yang, Y. (2018) Selective leaching of dissolved organic matter
628 from alpine permafrost soils on the Qinghai-Tibetan Plateau. J. Geophys. Res.
629 Biogeosci., 123, 1005-1016.
630 Ward, C. P. and Cory, R. M.(2015) Chemical composition of dissolved organic matter
631 draining permafrost soils. Geochim. Cosmochim. Acta 167, 63-79.
632 Ward, C.P. and Cory, R.M. (2016) Complete and Partial Photo-oxidation of Dissolved
633 Organic Matter Draining Permafrost Soils. Environ. Sci. Technol. 50, 3545-3553.
634 Weishaar, J.L., Aiken, G.R., Bergamaschi, B.A., Fram, M.S., Fujii, R. and Mopper, K.
635 (2003) Evaluation of specific ultraviolet absorbance as an indicator of the chemical
636 composition and reactivity of dissolved organic carbon. Environ. Sci. Technol. 37,
637 4702-4708.
638 Wickland, K.P., Aiken, G.R., Butler, K., Dornblaser, M.M., Spencer, R.G.M. and Striegl,
639 R.G. (2012) Biodegradability of dissolved organic carbon in the Yukon River and its
640 tributaries: Seasonality and importance of inorganic nitrogen. Global Biogeochem.
641 Cycles 26, doi:10.1029/2012GB004342.
642 Wild, B., Schnecker, J., Alves, R.J.E., Barsukov, P., Bárta, J., Čapek, P., Gentsch, N.,
643 Gittel, A., Guggenberger, G., Lashchinskiy, N., Mikutta, R., Rusalimova, O.,
644 Šantrůčková, H., Shibistova, O., Urich, T., Watzka, M., Zrazhevskaya, G. and Richter,

A. (2014) Input of easily available organic C and N stimulates microbial decomposition of soil organic matter in arctic permafrost soil. Soil Biol. Biochem. 75, 143-151.

Wu, G., Liu, Y., Zhang, Q., Duan, A., Wang, T., Wan, R., Liu, X., Li, W., Wang, Z. and Liang, X. (2007) The influence of mechanical and thermal forcing by the Tibetan Plateau on Asian climate. J. Hydrometeorol. 8, 770-789.

Yao, T., Pu, J., Lu, A., Wang, Y. and Yu, W. (2007) Recent glacial retreat and its impact on hydrological processes on the Tibetan Plateau, China, and surrounding regions. Arct. Antarct. Alp. Res. 39, 642-650.

Zhang, Z.Q. and Wu, Q.-B. (2012) Predicting changes of active layer thickness on the Qinghai-Tibet Plateau as climate warming. J. Glaciol. Geocryol. 34, 505-511.

Zhu, X., Wang, W. and Fraedrich, K. (2013) Future climate in the Tibetan Plateau from a statistical regional climate model. J. Clim. 26, 10125-10138.

Zimov, S.A., Schuur, E.A.G. and Chapin, F.S. (2006) Permafrost and the global carbon budget. Science 312, 1612-1613.

Figure and table captions

Fig. 1. Location of the QTP and sampling sites Q1 to Q20. Sites marked by a star were selected for FT-ICR MS or ^{14}C age analyses. The AL and PL denote the sampling locations of the active and permafrost layers. The blue line and the red line represent the first order and second order stream, respectively, and the blue dashed line denotes stream without GPS data.

Fig. 2. (a) Stream water discharge, (b) pH, and (c) conductivity at the sampling sites in 2015; and (d) DOC concentration in stream water and PL/AL leachates collected in 2015 (filled circles) and 2016 (open circles).

Fig. 3. UV-visible optical indices of the stream water and PL/AL leachate samples collected in 2015 (filled circles) and 2016 (open circles) on the QTP: $S_{275\text{-}295}$ (a) and $SUVA_{254}$ (b).

Fig. 4. Variations of ^{14}C age of HMW UDOM across the alpine stream spatially (a), and at headstream Q-1 temporally (b).

Fig. 5. van Krevelen diagrams of AL leachate DOM (a), PL leachate DOM (b), headstream DOM Q-1 (c), downstream DOM Q-17 (d), the relative abundance of defined compound class in different samples (e). CA = condensed aromatics, Pol. = polyphenols, Uns. = highly unsaturated compounds, Ali. = aliphatics, Pep. = peptides; and Sug. = Sugar. The van Krevelen plots of AL and PL leachate DOM was modified from Wang et al. (2018).

Fig. 6. (a) Relative contribution of AL leachate DOM to headstream DOM (Q-1); and (b) temporal variation of the DOC concentration at headstream Q-1.

Table 1 The number of molecular formulas assigned, modified aromaticity index (AI_{mod}), mean molecular weight (mean MW) and relative abundance of defined compound classes detected by FT-ICR MS for DOM samples from the QTP, including soil leachates (AL and PL) and stream waters (Q-1, Q-9 and Q-17). CA = condensed aromatics, Pol. = polyphenols, Uns. = highly unsaturated compounds, Ali. = aliphatic, Pep. = peptides. The molecule signatures of AL and PL leachate DOM can also be found in Wang et al. (2018).

Table 2 The number of specific molecules identified in the AL leachate DOM and the PL leachate DOM within the fluvial network, and the change in the relative abundance of each formula during the transportation.

Supplementary Figure S1. Van Krevelen diagrams showing the molecular changes of DOM from head to down-stream on the QTP. The blue and red dots denote decreasing trends and increasing trends, respectively. The color gradient shows the percentage of change. The lines separating compound categories [a]aliphatics and peptides [b] highly unsaturated compounds [c] polyphenols [d] condensed aromatics based on rules in the methods are just for visualization, and the exact categorization may differ.

Supplementary Table S1. Radiocarbon data for HMW UDOM from AL, PL and site Q-1.

701 Fig. 1

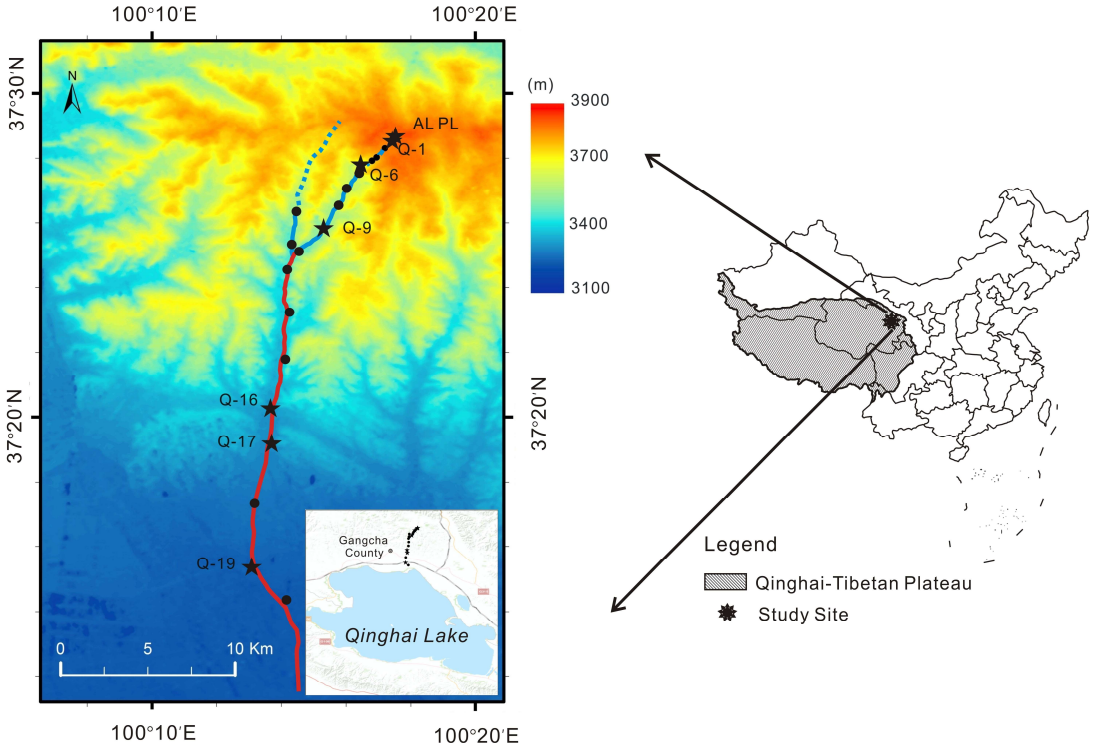

702

703

704 Fig. 2

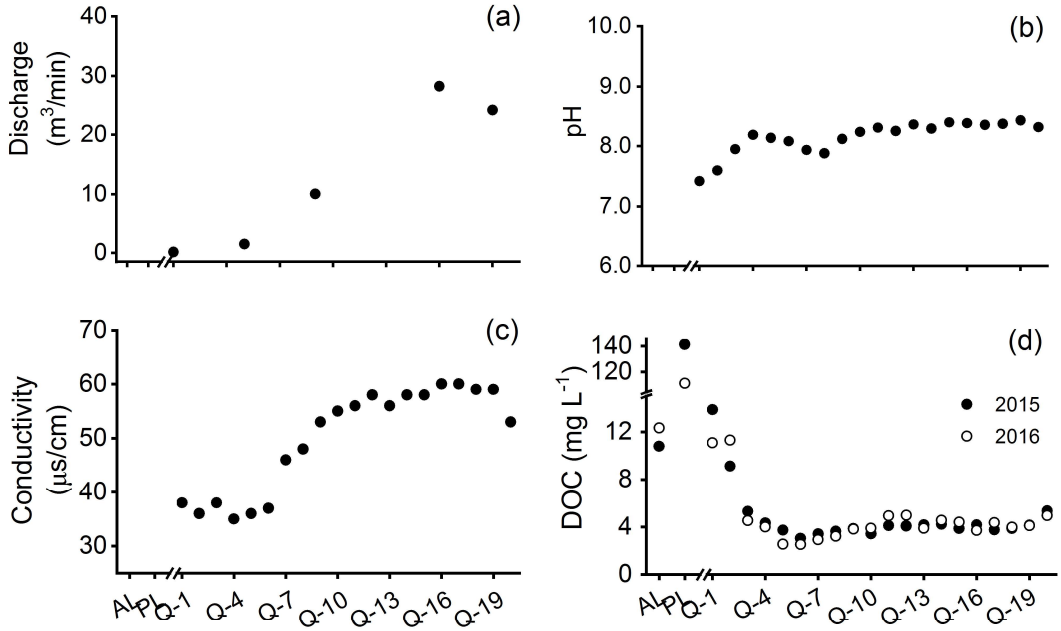

705

706

707 Fig. 3

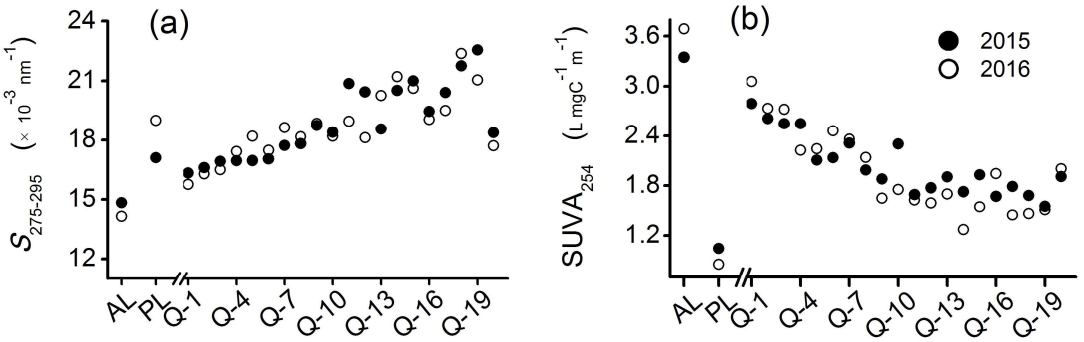

708

709

710 Fig. 4

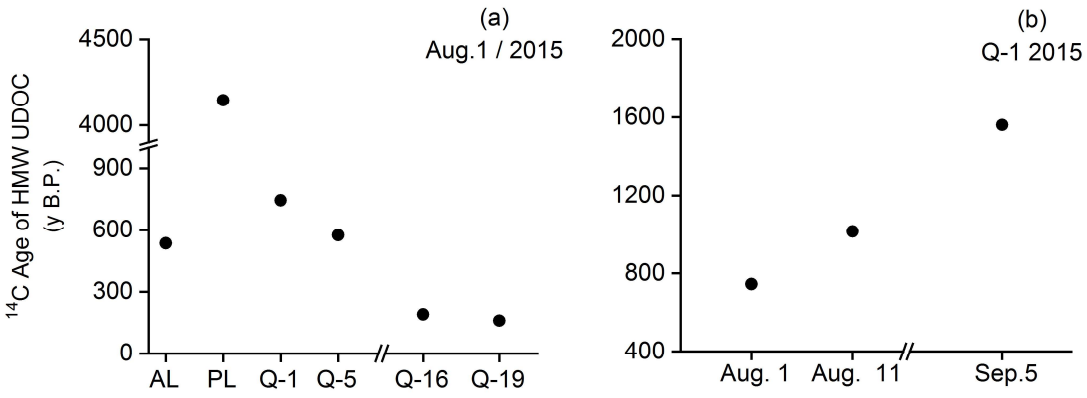

711

712

713 Fig. 5

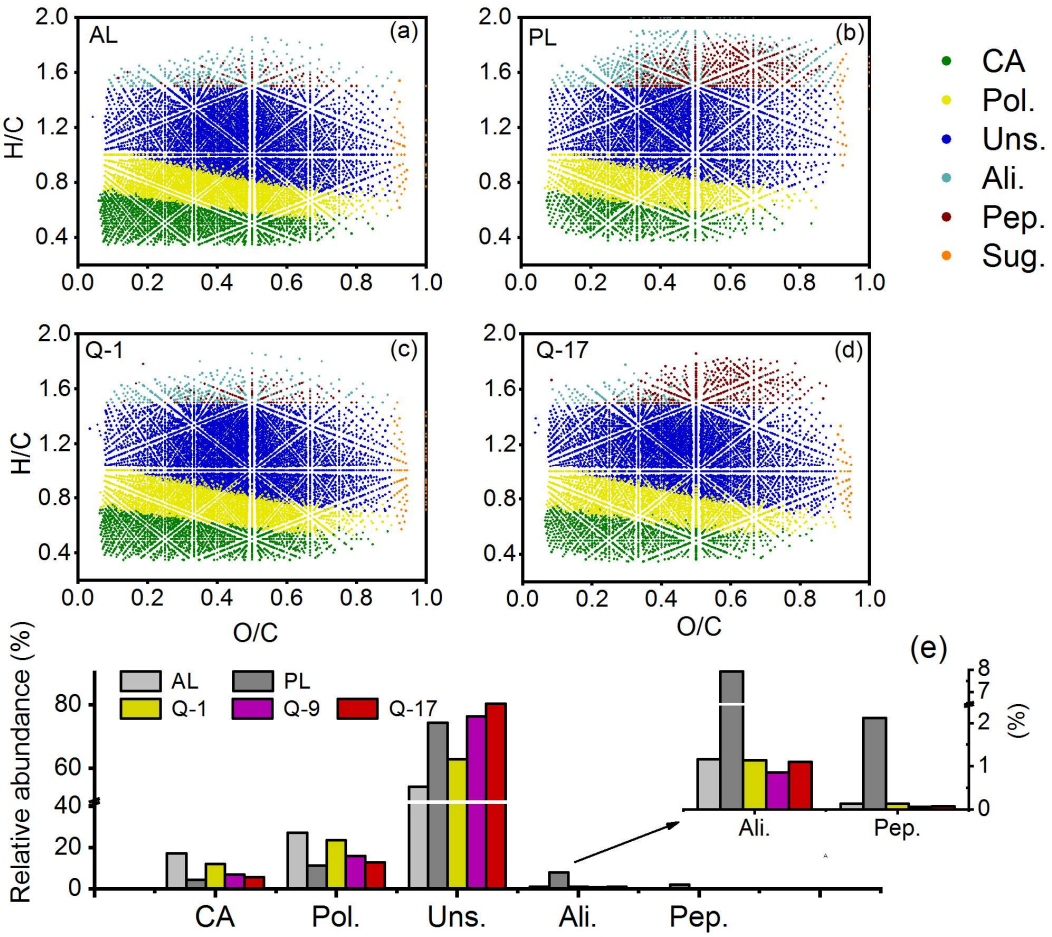

714

715

716 Fig. 6

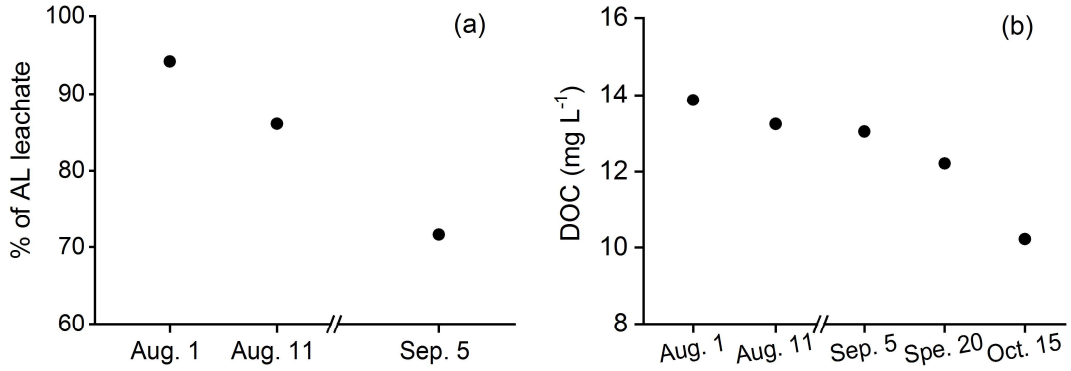

717

718

719 **Table 1.**

720

Sample	Formulas assigned	Mean MW	AI_{mod}	CA (%)	Pol. (%)	Uns. (%)	Ali. (%)	Pep. (%)
AL	14709	498.81	0.47	17.23	27.10	54.28	1.16	0.14
PL	9645	452.73	0.30	4.32	11.33	74.23	7.92	2.12
Q-1	14924	510.07	0.43	12.05	23.69	62.85	1.14	0.14
Q-9	11724	500.19	0.38	6.86	15.82	76.32	0.86	0.06
Q-17	11074	486.50	0.36	5.53	12.91	80.31	1.11	0.08

721

722

723 **Table 2:**

724

Samples		All Formulas	Only CHO	Contains N	Contains S	Contains N& S	Condensed aromatics	Polyhoenols	Unsatuated	Aliphatics	Peptides
AL specific	AL	6409	1793	3370	424	822	1620	1720	2970	38	23
	Q-1	5311 (17%)	1653 (8%)	2791 (17%)	349 (18%)	517 (37%)	1278 (21%)	1416 (18%)	2549 (14%)	20 (47%)	14 (39%)
	Q-9	3365 (47%)	1294 (28%)	1917 (43%)	153 (64%)	0 (100%)	748 (54%)	838 (51%)	1759 (41%)	6 (84%)	1 (96%)
	Q-17	2623 (59%)	985 (45%)	1570 (53%)	67 (84%)	0 (100%)	550 (66%)	602 (65%)	1453 (51%)	5 (87%)	0 (100%)
PL specific	PL	1345	515	551	278	0	2	23	318	597	385
	Q-1	222 (83%)	90 (83%)	102 (81%)	30 (89%)	0	0 (100%)	11 (52%)	126 (60%)	46 (92%)	36 (91%)
	Q-9	117 (91%)	44 (91%)	46 (92%)	27 (90%)	0	2 (0%)	14 (39%)	96 (70%)	1 (100%)	4 (99%)
	Q-17	130 (90%)	47 (91%)	55 (90%)	28 (90%)	0	2 (0%)	13 (43%)	104 (67%)	6 (99%)	5 (99%)

Figure S1.

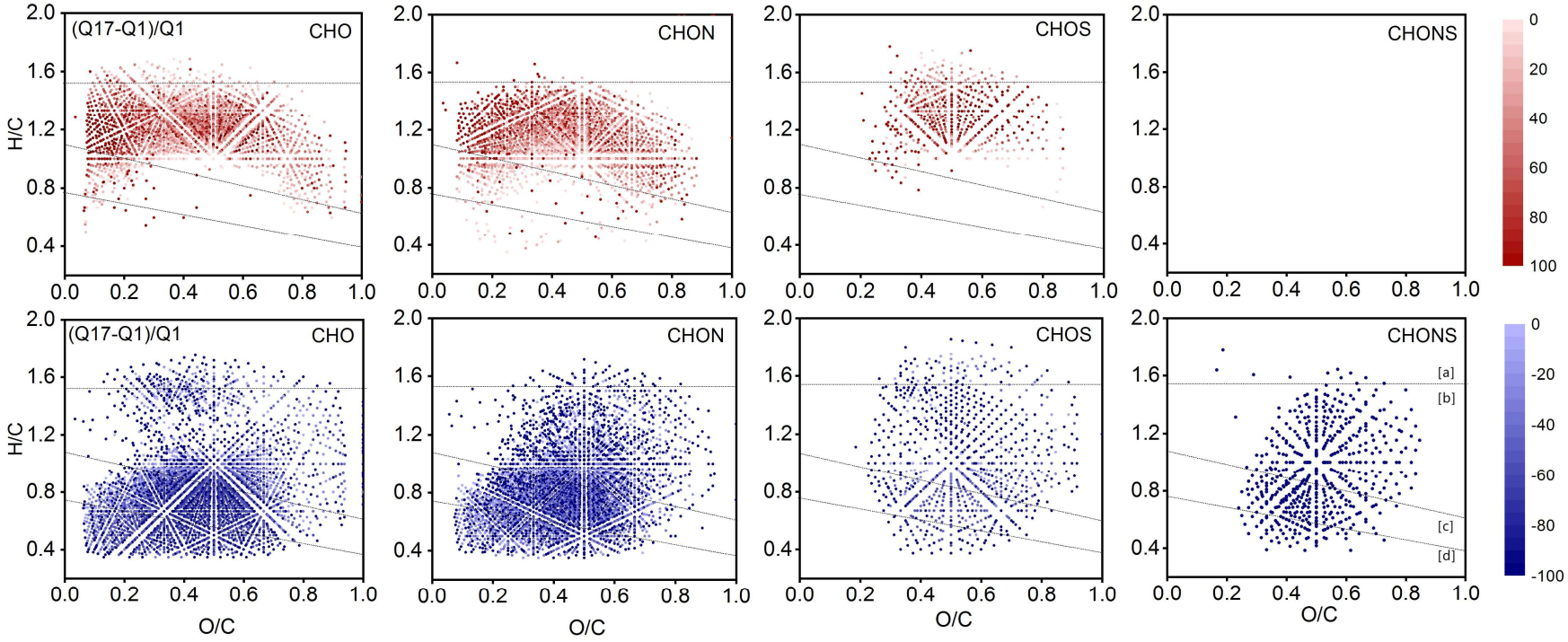
(Q17-Q1)/Q1
CHO
CHON
CHOS
CHONS
H/C
O/C
[a]
[b]
[c]
[d]
0
20
40
60
80
100
-20
-40
-60
-80
-100

727 **Table S1:**

Time	Fraction of modern standard	±	$\Delta^{14}C$(‰)	±	^{14}C age (yr BP)	±
AL	0.9358	0.0015	-64.2	1.5	535	15
PL	0.5971	0.0010	-402.9	1.0	4145	15
Q-1 Aug. 1	0.9116	0.0015	-88.4	1.5	745	15
Q-1 Aug. 11	0.8816	0.0014	-118.4	1.4	1015	15
Q-1 Sep.5	0.8233	0.0014	-176.7	1.4	1560	15

728

729